Chromogenic mechanisms in blue-and-white porcelains

Ariane Pinto, Jesse Groenen, Bing Zhao, Tiequan Zhu, Philippe Sciau

Chromogenic mechanisms in blue-and-white porcelains

Ariane PINTO[a*1], Jesse GROENEN[a], Bing ZHAO[c], Tiequan ZHU[def], Philippe SCIAU[a*]

[a] CEMES, Université de Toulouse, CNRS, 29 rue Jeanne Marvig, 31055, Toulouse, France

[b] CRCAO UMR 8155, CNRS, 52 Rue du Cardinal Lemoine, 75005 Paris, France

[c] School of Sociology and Anthropology of Sun Yat-sen University, 135 Xigangxi Road, Guangzhou 510275, China

[d] Southern Marine Science and Engineering Guangdong Laboratory (Zhuhai) Zhuhai, 519000, China

[e] The Joint Research Center of Maritime Silk Road by Sun Yat-sen University and Yangjiang Municipal Government, Yangjiang, 529500, China

* *Corresponding authors: ariane.pinto@cea.fr; philippe.sciau@cemes.fr*

Abstract

The blue underglaze decorations of Chinese blue-and-white porcelains are due to the use of a cobalt-based blue pigment. Nevertheless, for a same time period and production centre, wares can present wide colour variations in both hue and intensity. Fourteen Ming samples were investigated using colorimetry, Raman spectroscopy and SEM-EDS, in order to better understand the origin of these variations. The majority of the sherds dates back to the middle 15th- early 16th century. The chromogenic mechanism of the hue and intensity variations appears to be complex and multifactorial. Six main factors have been identified: the elemental composition of the pigment particles, in particular the Fe/Co ratio, the pigment spinel structure, the size as well as the distribution of the colouring particles, the environment of the pigment particles and the colour of the glaze.

Keywords

Chinese porcelains; Blue pigment; Spinel; Cobalt aluminate; Raman spectroscopy

Introduction

Blue colour holds a special dimension in many civilisations for its association with calm, peace or natural environments such as sky or water [1]. Natural blue colouring agents are also very rare. Blue colour was mostly obtained from expensive Lapis-Lazuli or cobalt oxides, or produced as a synthetic pigment from copper minerals (e.g. Egyptian blue) [2]. In the case of Chinese blue-and-white porcelain, famous around the world for the finesse of its blue decorations contrasting with the white body, a cobalt-based pigment was applied on the ware before glazing. After one-step firing at high temperature (1250-1300°C), it resulted in underglaze blue decorations [3]. Blue-and-white porcelain manufacturing process is well mastered since the Yuan Dynasty (1279-1368 AD) and the production

[1] Present adress : Arc Nucléart, CEA Grenoble, 17 avenue des Martyrs, 38054 GRENOBLE Cedex 9

become massive under the Ming Dynasty (1368-1644 AD) [3]. However, productions from the same time period and production centre show blue decorations with significant colour variations both in hue (vivid blue to greenish blue) and intensity (dark to light blue) (**Fig. 1**).

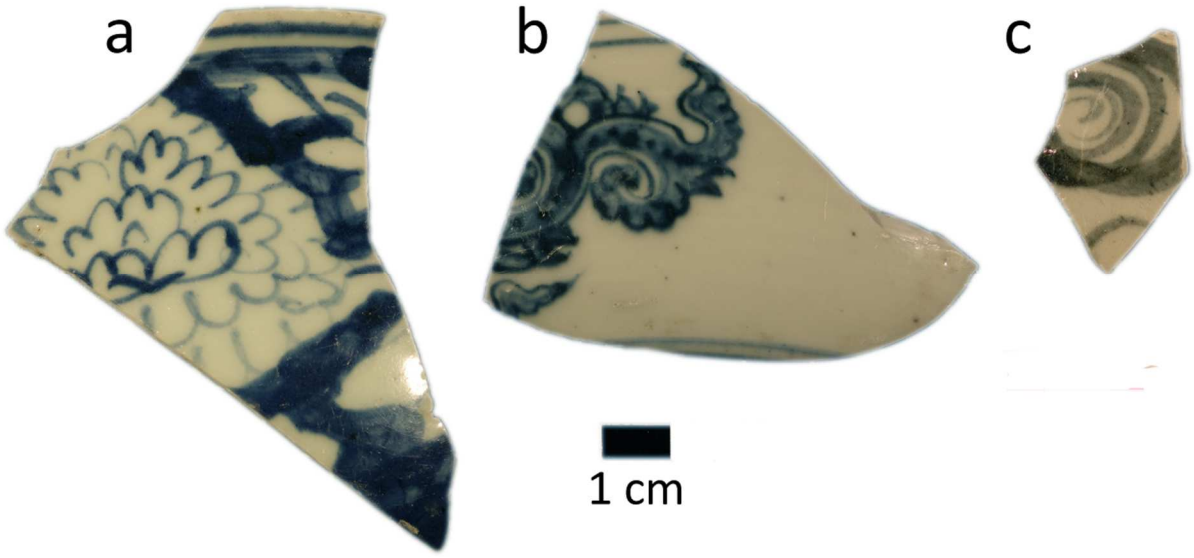

Figure 1 : Different blue decoration hues on Ming samples. (a) Sample TZ09: vivid blue. (b) Sample TZ06: greenish blue. (c) Sample TZ07: grey.

Numerous researches have been dedicated to the chromogenic mechanisms at the origin of these colour variations [4]. For a long time, the chemical composition of the pigment and the concentration of transition elements (Co, Fe, Mn) were considered main parameters in the hue variation [5-10]. In their study on Yuan Dynasty productions (1279-1368 AD), Tiequan ZHU *et al.* [9] correlated the colour variation to Co/Fe and Co/Mn ratios. On Ming Dynasty productions (1368-1644 AD), light blue and dark blue show different Mn/Co and Fe/Co ratios, dark blue zones being richer in Mn with respect to iron [6-7].

Different studies on the pigment zone showed the presence of Co-based phases, including $CoAl_2O_4$ and CoO [11-14]. They have a direct impact on the blue colour, but their connection with the hue variation was not clearly established [4]. Furthermore, some studies highlighted the presence of acicular crystals of anorthite ($CaAl_2Si_2O_8$) surrounding the Co-based phases and mentioned a potential role in the chromogenic process [13,15]. Finally, on the surface of the glaze, the formation of Fe and Mn-rich phases (Fe_2O_3, Fe_3O_4, Mn_3O_4) are also responsible for the darkening of the blue decorations [16].

In most of the previous studies, the composition of cobalt pigment and the Co-based phases were identified through the glaze. Its thickness inevitably induces a loss of information regarding the size, concentration and distribution of pigment underglaze crystals [4]. Therefore, previous studies can be contradictory due to the complexity of the pigment zone and its inaccessibility. In this study, we took advantage of a corpus of fourteen samples produced during the Ming Dynasty, between the middle of the 15th and early 17th century. We combine two approaches. Firstly, we performed colorimetric measurements at the surface of the samples. Secondly, we carried out elementary and microstructural analysis on cross-sections cut at the exact location of the surface measurements. Then, we were able to connect the colour seen by the naked eye to the underglaze microstructure and to uncover crucial parameters explaining the shade variation.

Samples and method

2.1 Samples description and preparation

All the studied samples have been excavated from the urban site of Maojiawang (Xichengqu district, Beijing municipality). This pit of 8.3 meters long and 5.6 meters wide, excavated in 2005, has yielded more than 100,000 fragments of ceramics originated from 20 kilns sites in China [17]. According to stylistic study, the fourteen samples studied were produced at Jingdezhen and surrounding area (Jiangxi Province). They can be dated from the middle and late Ming Dynasty (middle 15th-early 17th century) and the majority of sherds is dated from the middle 15th-early 16th century. They were provided by the Beijing Archaeological Institute through Pr. Tiequan Zhu (Archaeometry Lab, Sun Yat-Sen University, Guangzhou). Descriptions and illustrations of samples are presented in **Appendices** (**A.1** and **Table A.2**).

In order to obtain objective data to compare the different blue variations we used colorimetry. Measurements were carried out on the surface of the wares and yielded different colour groups. Among these groups, nine representative samples (TZ05, TZ07, TZ08, TZ09, TZ10, TZ12, TZ16, TZ19, TZ20) were selected and cut on the exact location of the colorimetric measurements to gain access to the underglaze microstructure. The other five sherds were not cut because of the size of the fragments and the place of the colorimetry measurements. Sampling would have been too damaging for the sherds. The obtained cuts were mounted in epoxy resin and polished to obtain clean cross-sections.

2.2 Colorimetry

Colours of blue and white zones were measured on the surface of the wares using a Konica Minolta CM-700d spectrometer with a 10° angle. For each measurement, data for specular components included (SCI) and excluded (SCE) were taken simultaneously. We used a 3 mm aperture to adapt to small zones. Each zone underwent 3 to 5 measurements. Mean value of measurements are presented in **Appendices** (**Table A.3**). The colorimetric data was exploited using the CIELab 1976 system. Each colour is defined by three values: a* expresses the green (-100) and red (+100) components, b* the blue (-100) and yellow (+100) components and L* the brightness between black (0) and white (100).

2.3 Micro-Raman spectrometry

Micro-Raman spectrometry was performed on cross-sections at room temperature using a Xplora MV 2000 Horiba spectrometer with a solid-state laser excited at 532 nm; this single grating set-up equipped with an edge filter to eliminate elastic scattering has a high optical throughput, enabling high sensitivity with short acquisition times. The spectrometer is equipped with 100× microscope objectives, confocal set-ups and charge coupled device detectors.

2.4 Scanning electron microscopy

The electron microscopy investigations were performed on cross-sections using a scanning electron microscope (JEOL JSM 6490) equipped with an energy-dispersive X-ray spectrometer (SEM-EDS)

(IncaPentaFet X3). Both imaging and elemental analyses were performed in HV (*high vacuum*) mode, working distance 10 mm. The imaging was performed in backscattered electron mode. The electron acceleration was 15 kV for imaging and elemental analysis. Since ceramics are not conductive, a thin layer of carbon covered the cross-sections, in order to avoid any charging effect during the measurements.

Results

3.1 Colorimetry

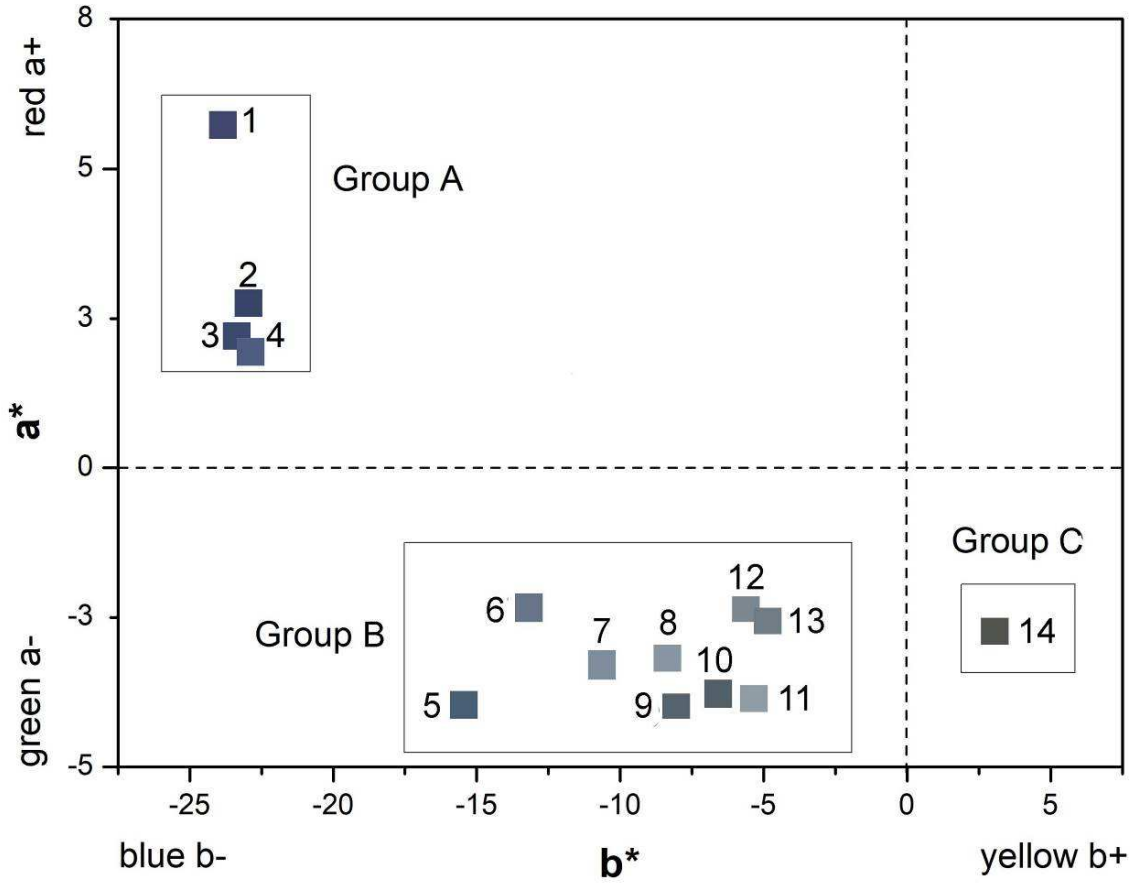

Figure 2 : Chromatic diagram of blue decorations. Only a* and b* values are showed. The colour corresponding to L*a*b* values are reported at the location of each point.
Group A: (1) TZ08; (2) TZ09; (3) TZ10; (4) TZ11;
Group B: (5) TZ21; (6) TZ14; (7) TZ12; (8) TZ16; (9) TZ05; (10) TZ06; (11) TZ19; (12) TZ20; (13) TZ13,
Group C: (14) TZ07.

The colorimetric measurements on blue decorations are presented in **Appendices** (**Table A.3)** and synthesized in **Fig. 2**. Based on the a* and b* values, we defined three groups. *Group A* includes four samples (TZ08, TZ09, TZ10, TZ11). The colorimetric values are characterized by a negative b* and a positive a* value corresponding to a vivid slightly purplish blue. This group contains the more vivid blue samples with a b* value below -21. *Group B* includes nine samples (TZ05, TZ06, TZ12, TZ13,

TZ14, TZ16, TZ19, TZ20, TZ21). The colorimetric values are characterized by negative a* and b* values corresponding to a dull slightly greenish blue. *Group C* is constituted of a single sample (TZ07) with a negative a* and a positive b* value. The blue decoration appears grey.

The colorimetric measurements on the white zones, without decorations, are presented in **Appendices** (**Table A.3)** and synthesised in **Fig. 3**. The transparent glaze is not perfectly colourless. The a* and b* values point to a yellow-greenish colour.

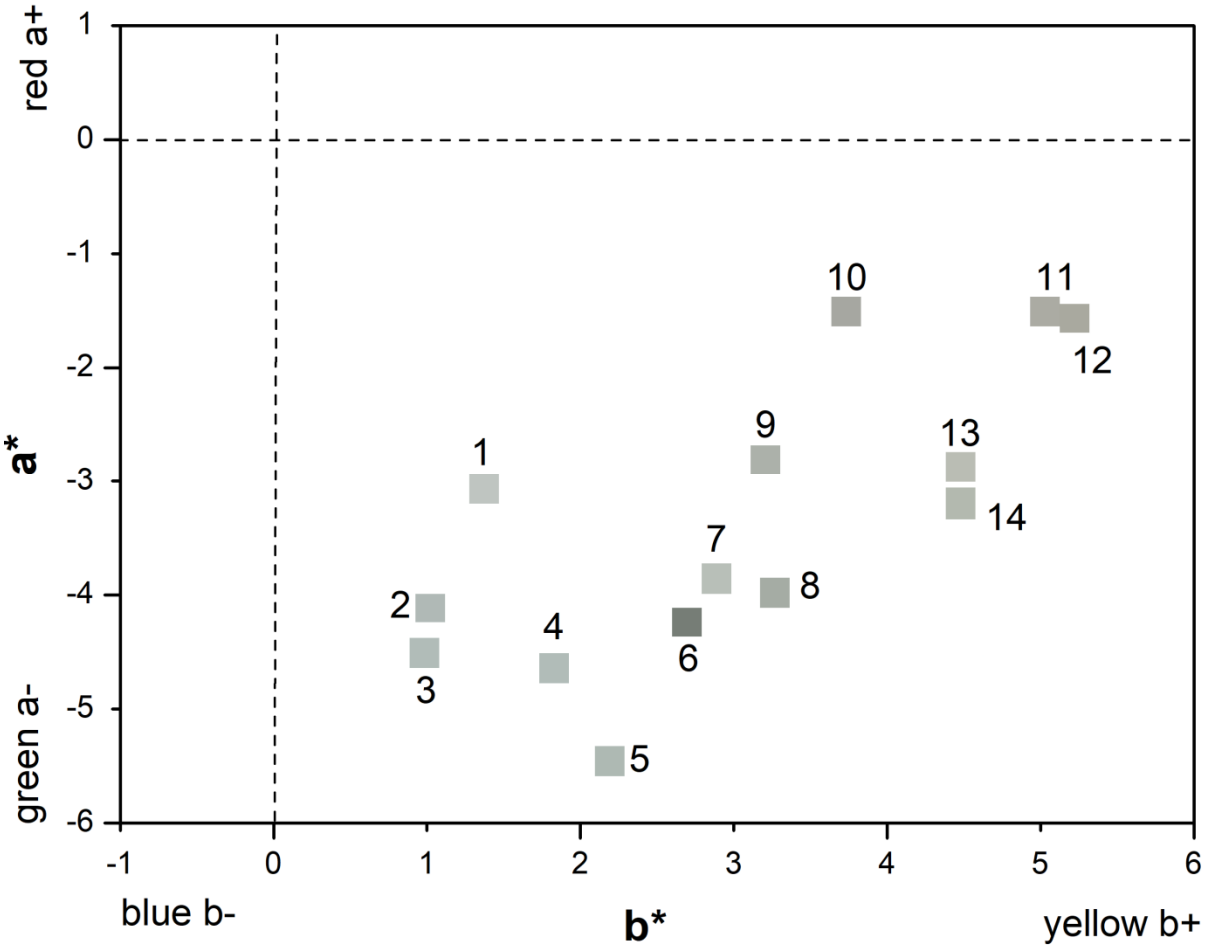

Figure 3 : Chromatic diagram of white zones. Only a* and b* values are showed. The colour corresponding to L*a*b* values are reported at the location of each point. (1) TZ10; (2) TZ09; (3) TZ11; (4) TZ19; (5) TZ20; (6) TZ08; (7) TZ12; (8) TZ13; (9) TZ14; (10) TZ07; (11) TZ06; (12) TZ05; (13) TZ16; (14) TZ21.

3.2 Observations

Pigment zone observations, performed on cross-sections, show similar microstructure with both crystalline and amorphous phases. On **Fig. 4a** the bright pigment particles are surrounded by a thick layer of acicular crystals. This type of microstructure was already spotted in multiple studies on blue-and-white porcelains dated from the Ming Dynasty [13,15].

Fig. 4b shows examples of a blue decoration zone presenting no pigment particle. The glaze is directly in contact with the body, but the pigment zone appears, in chemical contrast, lighter than the glaze indicating a different chemical composition. This different composition is most likely due to high concentration of transitional elements (Mn, Fe, Co) resulting from the pigment dissolution in the

glaze. Previous studies showed the possible absence of a specific zone containing pigment particles and anorthite crystals between the glaze and the body, where transition elements have completely diffused into the glaze [4,11]. In these cases, Co^{2+} ions react in tetrahedral coordination with the glaze network, leading to a blue colour. However, due to its lower tinting contribution, the density of color is lower [4]. Wang *et al*. also indicate that Fe ions in the glaze have no significant role in the color and Mn ions can have an influence on the darkening rather than on the hue [4].

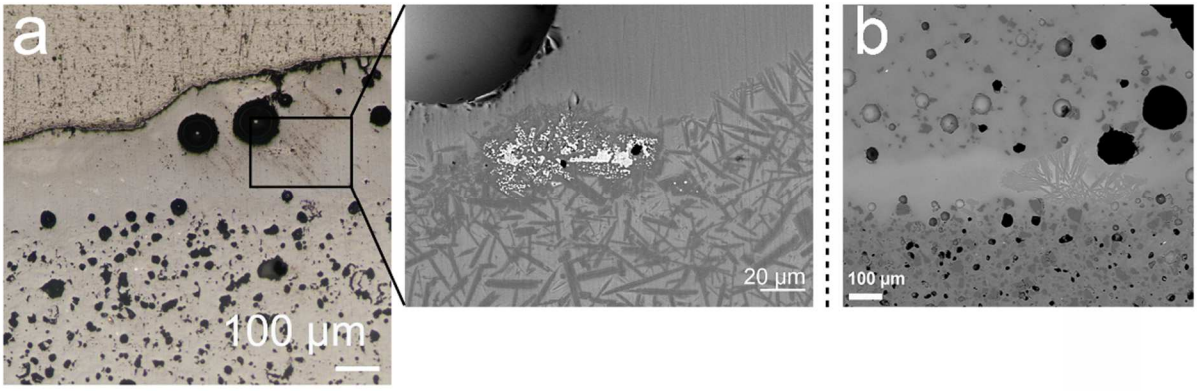

Figure 4 : Microstructures of the pigment zones. (a) With crystalline structures (optical and SEM images), sample TZ02; (b) Without pigment particle (SEM images), sample TZ20.

3.3 Micro-Raman spectrometry

Bright pigment particles and acicular crystals were investigated using micro-Raman spectrometry. Raman spectrum measured on pigment particles are displayed in **Fig. 5**. Spectra are characterized by six peaks, with positions and relative intensities that are consistent with the Raman spectrum of cubic spinels, more precisely aluminates with the general formula AAl_2O_4 [18]. The partially inverse structure of some aluminates ($CoAl_2O_4$, $FeAl_2O_4$, $MnAl_2O_4$, $MgAl_2O_4$) can cause the activation of additional Raman modes, in particular a second A_{1g} mode between 699 et 720 cm^{-1} noted as A_{1g}* [18].

Fig. 5 shows three groups of spectra. *Group 1* spectra are defined by large and less pronounced peaks dominated by an A_{1g} mode, between 739 and 763 cm^{-1}. They can be discriminated by a small $F_{2g}(1)$ mode. *Group 2* spectra are similar to *Group 3* spectra, with a dominant A_{1g} mode between 748-754 cm^{-1}, but they can be discriminated by an A_{1g}* mode distinct from the main A_{1g} mode and a $F_{2g}(1)$ mode more intense. *Group 3* spectra are similar to *Group 2* spectra because of an intense $F_{2g}(1)$ mode, as the dominant mode, but the $F_{2g}(2)$ and A_{1g} modes have the same intensity and are more intense than $F_{2g}(3)$ mode. From the modes' relative intensity and positions, *Group 1* spectra are close to hercynite ($FeAl_2O_4$) references [18-19]. *Group 2* spectra have an intense $F_{2g}(1)$ mode, more characteristic of galaxite ($MnAl_2O_4$) and cobalt aluminate ($CoAl_2O_4$) [14,18,20]. The relative intensity of *Group 3* spectra Raman modes is close to $MnAl_2O_4$, but the positions of $F_{2g}(1)$, E_g, $F_{2g}(2)$ and A_{1g} modes are closer to those reported for $CoAl_2O_4$ [18,20].

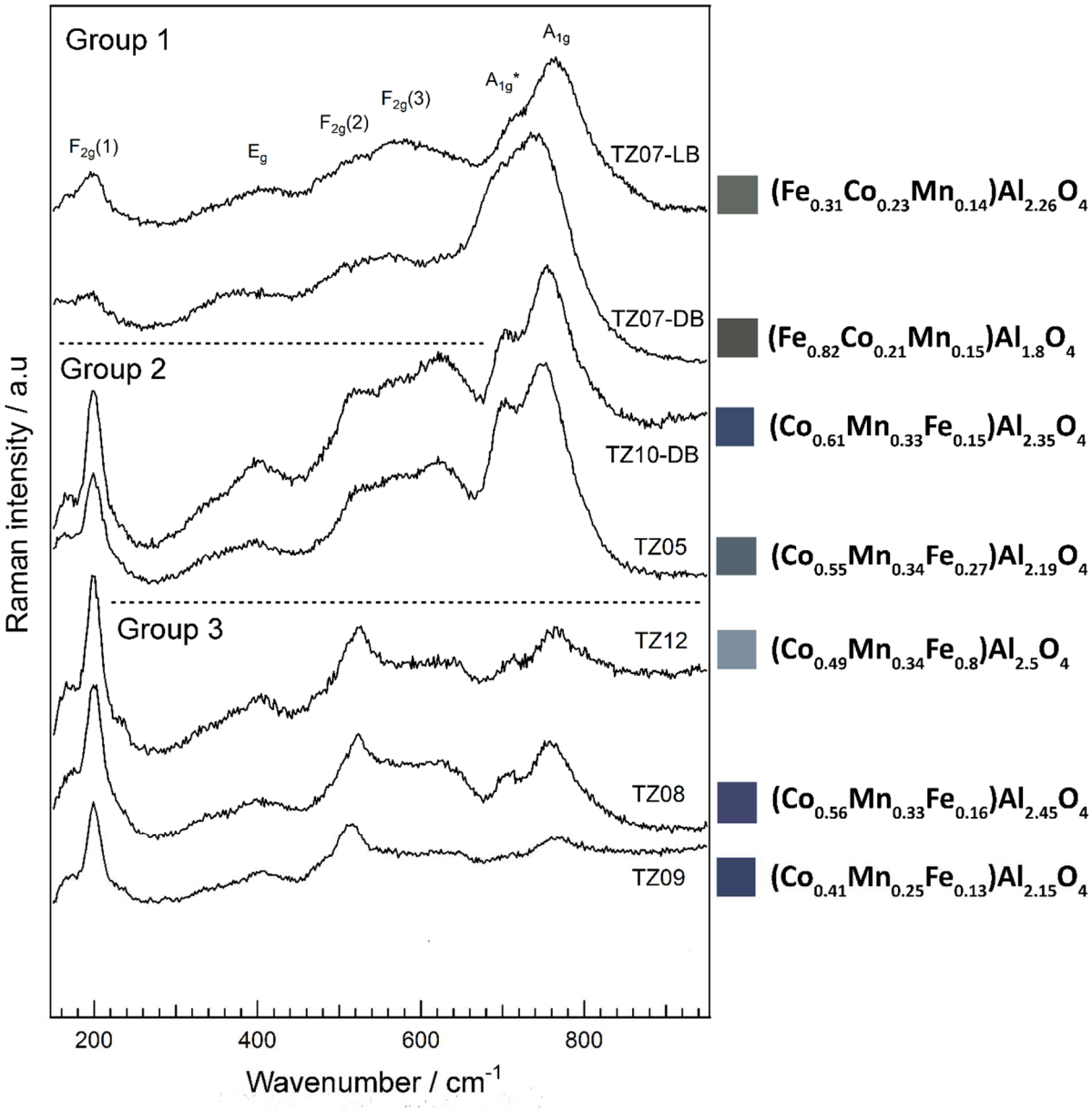

Figure 5 : Raman spectra measured on pigment particles. For each Raman spectrum, we also indicate the chemical formula calculated from the SEM-EDS point measured on the same location and the surface colour measured by colorimetry. DB for Dark Blue and LB for Light Blue zones.

Acicular crystals were identified as anorthite ($CaAl_2Si_2O_8$) from their Raman spectra thank to the dominant double peak at 479 and 506 cm^{-1}, and four less intense peaks at 191, 278, 406 et 561 cm^{-1} [21] (spectra shown in **Appendice Fig. A.4**).

3.4 SEM-EDS

The different types of aluminates are hard to distinguish from their Raman spectra because the differences in the E_g, $F_{2g}(2)$ and A_{1g} wavenumbers do not exceed 3-4% [18]. SEM-EDS provided the chemical composition at the same spot as the micro-Raman spectrometry analysis. All the points studied are illustrated in **Appendice A.5.** The complete chemical compositions are presented in **Appendices (Table A.6)**. From these compositions we calculated a formula based on aluminates

structure (AAl_2O_4), where *A* can be Co, Fe and Mn. The calculated chemical formulas corresponding to each Raman spectrum are outlined on **Fig. 5**.

Although micro-Raman spectrometry distinguished three groups, calculated chemical formulas are only of two types: a composition closer to hercynite ($FeAl_2O_4$) with Co and Mn substitution (TZ07), and a chemical composition close to cobalt aluminate ($CoAl_2O_4$) with more or less Mn and Fe substitutions (TZ05, TZ08, TZ09, TZ10, TZ12). The presence of cobalt aluminate ($CoAl_2O_4$) as a blue pigment in blue-and-white porcelains was widely reported these two last decades [7,13-14,22-26].

Chemical substitutions (Mn, Fe, Co, Ni, Mg) are due to the existence of solid-solutions between $CoAl_2O_4$, $FeAl_2O_4$ and $MnAl_2O_4$. Co^{2+}, Fe^{2+} and Mn^{2+} mostly adopt tetrahedral coordination, which eases the substitutions. Mg can also be present as substitutions and sample TZ16 even shows a high Mg content, superior to cobalt (see **Table A.6**). TZ16 pigment particles belong to the solid-solution between $CoAl_2O_4$ and $MgAl_2O_4$, with the gradual substitution of Co^{2+} ions by Mg^{2+} ions on tetrahedral sites [27].

Discussion

4.1 Pigment chemical composition

The blue colour in blue-and-white porcelains is due to the use of cobalt. Co-rich minerals can cause blue colour when they are dissolved in siliceous glass, but other transition elements (Fe, Mn etc.) can also affect the final hue. **Table 1** shows the content of colouring elements (Mn, Fe, Co) in pigment grain depending on the L*, a* and b* parameters measured on the surface. The content of colouring elements was measured by SEM-EDS and is expressed in atomic percent (at%). Detailed compositions of pigment particles are presented in **Appendices** (**Table A.6)**.

TZ08, TZ09 and TZ10 samples are characterised by a high cobalt content. They are also part of the colour *Group A* with a negative b* parameter (-22.98 > b* > -23.96) correlated to a vivid blue. However, TZ05 (*Group B*) also shows a high cobalt rate, but the b* parameter indicates a less vivid blue and the a* parameter a greenish colour. Thus, the amount of cobalt is not the only parameter inducing the vividness of the blue.

The iron content also influences the vividness of the blue. *Group A* samples, with vivid blue decorations, also show low Fe/Co ratio (<0.30). The higher the Fe/Co ratio is, the higher the b* parameter is, causing a less vivid blue. A similar trend is observed in Vietnamese porcelains, where iron was probably added to modify the blue decoration from a vivid blue to a greenish one [5]. TZ07 (*Group C* sample) shows a high amount of iron (11.87 at%). It has a strong impact on the colour since this sample is the only one showing a positive b* parameter and a grey colour.

The manganese content does not appear to have any direct impact on the blue colour variation. Mn^{3+} ions in glass can produce a purple colour while Mn^{2+} is colourless. However, samples with a* parameter, connected to a slightly purplish colour, are not the ones with the higher Mn content or the ones with the higher Mn/Co ratio. Due to mainly reducing firing conditions, manganese is probably mostly in Mn^{2+} explaining its absence of impact on colour.

Colour Group	ID	Composition						Colorimetry		
		Co	Mn	Fe	Fe/Co	Mn/Co	Mn/Fe	*L**	*a**	*b**
A	**TZ08**	7.30	4.23	2.02	0.28	0.58	2.09	30.5	5.76	-23.96
	TZ10-DB	8.16	4.35	1.96	0.24	0.53	2.22	31.37	2.24	-23.47
	TZ09	5.65	3.36	1.71	0.30	0.59	1.96	29.55	2.77	-22.98
B	**TZ16**	4.71	2.57	1.71	0.36	0.55	1.50	61.78	-3.20	-8.35
	TZ05	7.24	4.54	3.55	0.49	0.63	1.28	41.4	-3.99	-8.09
	TZ20	5.29	4.75	2.73	0.52	0.90	1.74	55.94	-2.37	-5.76
	TZ19	3.24	2.07	3.48	1.07	0.64	0.59	63.98	-3.84	-5.45
C	**TZ07-DB**	2.93	2.02	11.87	4.05	0.69	0.17	35.4	-2.66	3.18

Table 1 : Transition elements content (at%) in pigment particles and colorimetric measurements. The colour groups presented in Fig. 2 are also mentioned.

4.2 Pigment structure

The chromogenic mechanism of blue coloration is due not only to the type and relative amount of transition elements in the pigment. The oxidation state of metallic ions (valence) and the stereochemistry (coordination) are also key parameters.

As seen in the chemical formula shown in **Table A.6**, TZ02, TZ05, TZ08, TZ09, TZ10, TZ12 and TZ20's pigment particles have composition close to cobalt aluminate ($CoAl_2O_4$) but with Mn and Fe substitutions. Cobalt aluminate, also called 'cobalt blue', presents a vivid blue colour resulting from tetrahedral Co^{2+} electronic transitions leading to the characteristic absorption band at 550-680 nm [20,28-31]. Tetrahedral coordination of Co^{2+} ions is key to obtain an intense blue colour [32]. This was observed on TZ08, TZ09, TZ10 and TZ12. On **Fig. 5**, the Raman spectra show an intense $F_{2g}(1)$ mode which has been ascribed to the Co-O stretching vibration in tetrahedral coordination [20]. This proper coordination is obtained through a high synthesis temperature, typically between 1000°C and 1200°C [33]. The vivid blue colour of TZ08, TZ09 and TZ10 appears to be connected to substituted $CoAl_2O_4$ particles obtained at high firing temperature, with Co^{2+} in proper tetrahedral coordination.

However, numerous studies showed that $CoAl_2O_4$ colour depends largely on its composition, structure and annealing temperature [34-37]. For the same chemical composition, $CoAl_2O_4$ can show blue or green colour depending on structural disorder connected to the synthesis temperature [36-37]. According to Shiva Salem and Federica Bondioli [37], the green coloration is due to a partially inverse spinel structure, obtained at low temperature, where part of Co^{2+} ions occupy octahedral sites. In contrast, the vivid blue colour is the result of a normal spinel structure, synthesized at high temperature, with Co^{2+} on tetrahedral sites. On the Raman spectrum presented in their study, the 516 cm^{-1} peak is very intense for the blue $CoAl_2O_4$ and less visible for the green $CoAl_2O_4$. TZ05's Raman spectrum (**Fig. 5**) shows a less visible 516 cm^{-1} peak and an additional A_{1g}* mode attributed to spinel inversion [18]. Its greenish colour could then be explained by pigment grain with an inverse spinel structure and Co^{2+} ions on octahedral sites.

Sample TZ07 exhibits a grey colour due to the presence of hercynite ($FeAl_2O_4$) substituted with Mn and Co. This phase gives rise to a dark colour [38] explaining the unusual hue of the « blue » decoration. Hercynite formation in TZ07 is connected to the high amount of Fe in the pigment particles and the firing under reducing conditions.

Sample TZ16 exhibits a light blue and a unique composition of the pigment in the $MgAl_2O_4$-$CoAl_2O_4$ solid solution with Mn and Fe substitutions. Numerous studies have explored pigments with compositions in the $Co_xMg_{1-x}Al_2O_4$ solid solution [27,31,35,39-40]. It appears that Mg-substituted $CoAl_2O_4$ colour varies from light blue to dark blue with the increase of Co with respect to Mg [31,39]. In TZ16, the light blue colour could then be linked to a high amount of Mg (equal to Co) (**Table A.6**).

4.3 Size and distributions of particles

The pigment zones show different size and distribution of pigment particles. On SEM images, we selected an area of 100 x 75 µm and we performed a particle counting using Image J software (**Appendice A.7**). A threshold range is set to discriminate the objects of interest from the background, in particular the pigments particles from the glassy matrix and the acicular crystals. Eight samples were analysed (TZ08, TZ09, TZ10, TZ16, TZ19, TZ20). **Table A.8** shows the number of particles on the analysed zone, the average size of particles and the number of particles depending on their size.

In Tian WANG *et al*. [4], it appears that the number of cobalt aluminate particles influences the blue intensity, with dark blue decorations containing higher number of particles than light blue zones. In our case, the total number of particles measured on a 100 x 75 µm area ranges from 140 (TZ16) to 894 (TZ10). Samples presenting the more vivid blue (-22.98 > b* > -23.96) reveal a pigment zone with a high number of particles (TZ08, TZ09, TZ10). Likewise, some of the samples with the lightest blue decoration (-5.45 > b* > -8.35) show a pigment zone with a small number of particles (TZ16, TZ19, TZ05). However, this tendency is not systematic since TZ20 show a high number of particles (475) but a b* value characteristic of a lighter blue (b*= -5.76). Others parameters such as the environment of the colouring particles can explain this exception.

The average size of particles also plays a key role in the chromogenic process concerning both the hue and the colour intensity. The two samples with the more vivid blue (TZ08 and TZ10) show pigment zones with high particle average size (0.840 and 0.795 µm²). For TZ08, some pigment particles can even reach 50 µm². In contrast, pigment particle average size, in TZ16, TZ19, and TZ20 with less intense blue, do not exceed 0.305 µm². Similar observations can be made concerning the colour intensity defined by the L* value. **Fig. 6** shows the correlation between the L* value and the average size of particles. Except from TZ09, the lesser the average size of particles is, the higher is the L* value and lighter the colour. Nevertheless, TZ09 belongs to *Group A*, with the darker and more vivid blue hues, thanks to the amount of cobalt and the coordination of the $CoAl_2O_4$ spinel, as we have seen above.

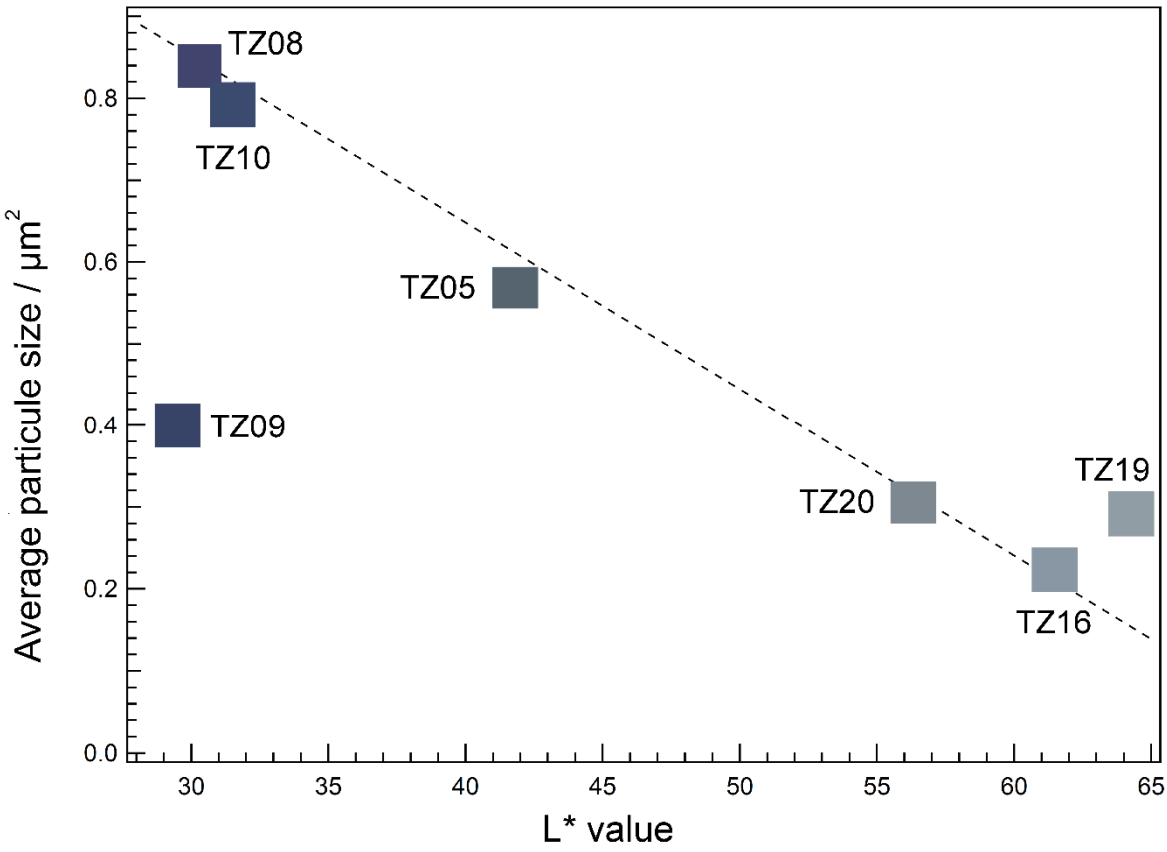

Figure 6 : Average particles size (µm²) in function of L* value (luminosity). The surface colour measured by colorimetry is also indicated.

4.4 Pigment particles environment

Ming samples pigment zones are also characterised by the presence of acicular crystals of anorthite surrounding the pigment particles. Several studies show a connexion between the density of anorthite crystals and the vividness of the blue [4,15]. According to Xiaochenyang Jiang *et al.* [15], the development of anorthite crystals during firing tends to act as a barrier coating to hinder the further dissolution of pigment particle and diffusion of cobalt ions. To verify if a thick anorthite layer is connected to a vivid blue, we studied eight pigment zones on seven samples (TZ05, TZ08, TZ09, TZ10-DB dark blue, TZ10-LB light blue, TZ16, TZ19, TZ20). **Fig. 7** shows the different pigment zones with three main tendencies.

Upper line samples (**Fig. 7a-b-c-d**) show the more vivid blue colours (22.98 < b*< - 23.96 for TZ08, TZ09, and TZ10-DB), as well as TZ05, which is greenish. All samples present a similar pigment zone with a thick layer (around the hundreds of microns) of acicular anorthite crystals surrounding the pigment particles. The glassy matrix between the anorthite crystals is lighter than the rest of the glaze, indicating that transition elements have diffused from the pigment particles. The upper line samples also include the darkest blue samples (29.55 < L*< 41.4). *A contrario,* the lower line (**Fig. 7e-f-g-h**) shows samples with the lightest blue (55 < L* < 62 for TZ16; TZ20, TZ10 LB, TZ19) characterized by the absence of a thick and homogeneous layer of anorthite crystals. TZ16 and TZ20 (**Fig. 7e-f)** present a “jumble” of anorthite crystals surrounding small pigment particles and no acicular crystals

can be seen for TZ10-LB and TZ19 (**Fig. 7g-h)**. Thus, a dark and vivid blue colour is directly connected to a dense and thick layer of anorthite crystals.

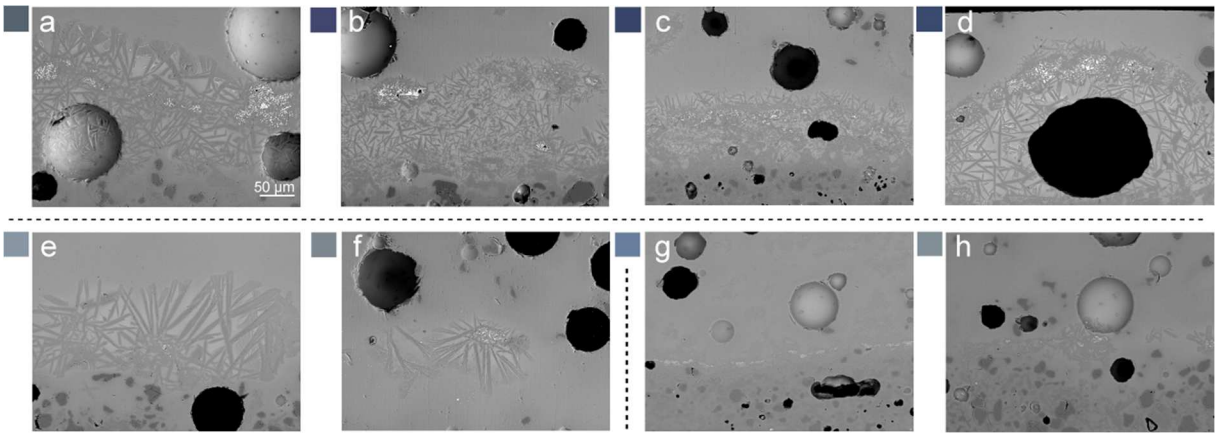

Figure 7 : Electronic images of pigment zones with crystalline structures. Polished cross-sections observed in BSE mode. The surface colours, measured by colorimetry, are also indicated. (a) TZ05; (b) TZ08; (c) TZ09; (d) TZ10-DB; (e) TZ16; (f) TZ20; (g) TZ10-LB; (h) TZ19.

Furthermore, sample TZ20 also exhibits blue decoration zones although no pigment particles are observed, as showed previously on **Fig. 4b**. Corresponding colorimetric measurements indicate a dull and light blue. In this case, the lack of intensity in the blue colour is more likely due to a partial dissolution of the pigment in the glassy matrix with the diffusion of the Co^{2+} ions above 900°C [41]. Similar phenomenon may have occurred for the lower line samples (**Fig. 7e-f-g-h**). The presence of a thin anorthite layer or no anorthite at all, allowed a partial dissolution of the pigment in the glassy matrix leading to small particle sizes and light and dull blue colours.

4.5 Glaze contribution

The white zone colorimetric analysis (**Fig. 3, Table A.3**) showed that glaze is not colourless. It can be slightly tinted in green-yellow or green-blue due to the presence of iron in ionic form. In glasses, Fe^{2+} gives a pale blue colour, whereas Fe^{3+} gives a yellow one [42]. Additional colours (amber, green-blue, brown) can be obtained with different Fe^{2+}/Fe^{3+} ratios [43]. Iron was not intentionally added as a colouring element, since blue-and-white porcelain used a colourless and translucent glaze, but it was present in the raw material. Because the glaze is put on the pigment, its coloration has an impact on the final blue coloration. It can reduce the vividness of the blue and create a greenish shade.

4.6 Summary

Samples from *Group A* present the more vivid and darker blue (b* > -22.98) and they all show the same pigment zone microstructure: numerous large pigment particles (average size > 0.4 µm²) comprised of cobalt aluminate ($CoAl_2O_4$) with lightly substituted with iron, surrounded by a thick layer of acicular anorthite crystals preventing their dissolution in the glassy matrix. TZ09 exhibits the lowest density of pigment grain and smallest average size, but the high cobalt content, the tetrahedral Co^{2+} coordination and the thick anorthite layer maintain a vivid blue colour.

Samples from *Group B* are characterized by a dull, greenish and lighter blue, but this colour hue may result from a wide variety of parameters. Not aiming to review group B, we exemplify this variety considering some representative samples:

- TZ05 has many parameters in common with *Group A* samples, such as the presence of $CoAl_2O_4$-type crystals, the size and number of colouring particles and the pigment zone microstructure with a thick anorthite layer. Nevertheless, pigment particles show a higher Fe/Co ratio than *Group A* samples and $CoAl_2O_4$ likely show an inverse spinel structure with Co^{2+} ions on the octahedral sites. In this case, the composition and structure of pigment particles lead to a greenish colour rather than a vivid blue one.
- TZ16 differs from other samples because of a singular pigment composition with a high amount of magnesium, leading to a light and dull blue colour.
- For TZ19 and TZ20, the light and dull blue colour is mainly attributed to small pigment particles and the lack of a thick layer of acicular anorthite crystals.

Finally, sample TZ07's grey (*Group C*) decorations are due to a high amount of iron in the pigment particles leading to the formation of hercynite ($FeAl_2O_4$) under the reducing conditions of firing.

The different parameters do not have the same impact on the colour. For instance, in the presence of large and numerous particles of cobalt aluminate, the colour of the glaze will not have a strong influence on the final colour. It will result in vivid dark blue decorations even if the glaze if coloured by Fe ions.

Conclusion

Combining surface colorimetric measurements and cross-section analysis using micro-Raman spectrometry and SEM-EDS proves to be truly insightful. We have shown that quantitative data and correlations can be assessed to identify the most relevant parameters involved in chromogenic mechanisms in blue-and-white porcelains. Multiple factors impact the blue colour variation with a complex interplay between parameters such as the chemical and structural composition of the pigment, the size and distribution of pigment particles, their environment and the glaze colour. In addition, our analysis provides information relevant to technical processes used in order to design the blue-and-white porcelain decorations.

From a technical perspective, obtaining a dark and vivid blue colour requires a pigment zone microstructure containing numerous large crystals of weakly substituted cobalt-aluminate, surrounded by a thick layer of acicular anorthite crystals. In order to achieve that, Chinese potters needed to master the purification and the high-temperature formation of the cobalt aluminate as well as insure the formation of the anorthite layer. For instance, insufficient purification of the cobalt preparation would lead to the formation of cobalt aluminate crystals strongly substituted with iron, or even dark-grey hercynite crystals in the most iron-rich environments.

From a historical point of view, the wide variation in blue colour cannot be correlated to any time period within the Middle and Late Ming Dynasty (middle 15th- early 17th century). The manufacturing process does not seem to undergo any significant change. A wide range of blue colour was therefore

obtained under different reigns through chemical and microstructural variations. These subtle shades of blue give this famous porcelain production its authentic charm.

Acknowledgments

The authors gratefully acknowledge Sébastien Moyano and Frédéric Neumayer (CEMES, Toulouse) for their technical assistance during the Raman spectroscopy experiments, as well as Christophe Deshayes (CEMES, Toulouse) for his assistance during the SEM-EDS experiments. They also acknowledge Guirec Ollivier, Luc Robbiola and the TRACES laboratory (University Toulouse-Jean Jaurès, Toulouse) for their assistance with the colorimetric measurements. This work was supported by the PHC CAI YUANPEI 2016-2018 program No. 36708RD.

Bibliography

[1] Pastoureau M. Blue: the History of a Color. Princeton: Princeton University Press, 2001.

[2] Zucchiati A, Bouquillon A, Katona I., D'Alessandro A. The 'Della Robbia blue': a case study for the use of cobalt pigments in ceramics during the Italian Renaissance. Archaeometry 2006; 48: 131-152. https://doi.org/10.1111/j.1475-4754.2006.00247.x

[3] Li Z, Bower VL , Li H. Chinese Ceramics: From the Paleolithic Period through the Qing Dynasty (The Culture & Civilization of China). New Heaven: Yale University Press, 2010.

[4] Wang T, Zhu T, Feng Y, Fayard B, Pouyet E, Cotte M, De Nolf W, Salomé M, Sciau, P. Synchrotron radiation-based multi-analytical approach for studying underglaze color: The microstructure of Chinese Qinghua blue decors (Ming dynasty). Anal Chim Acta 2016*;* 928: 20-31. https://doi.org/10.1016/j.aca.2016.04.053

[5] Colomban P, Sagon G, Huy L, Liem N, Mazerolles, L. Vietnamese (15th century) blue-and-white, Tam Thai and lustre porcelains/stonewares: glaze composition and decoration techniques. Archaeometry 2004*;* 46: 125-136. https://doi.org/10.1111/j.1475-4754.2004.00148.x

[6] Wen R, Wang C, Mao Z, Huang Y, Pollard A. The chemical composition of blue pigment on Chinese blue-and-white porcelain of the Yuan and Ming. Archaeometry 2007; 49: 101-115. https://doi.org/10.1111/j.1475-4754.2007.00290.x

[7] Coutinho M, Muralha V, Mirão J, Veiga J. Non-destructive characterization of oriental porcelain glazes and blue underglaze pigments using μ-EDXRF, μ-Raman and VP-SEM. Appl Phys A 2014, 114: 695-703. https://doi.org/10.1007/s00339-013-8147-8

[8] Simsek G, Colomban P, Wong S, Zhao B, Rougeulle A, Liem N. Toward a fast non-destructive identification of pottery: The sourcing of 14th-16th century Vietnameseand Chinese ceramic shards. J Cult Herit 2015; 16: 159-172. https://doi.org/0.1016/j.culher.2014.03.003

[9] Zhu T, Ding X, Kusimba C, Feng, Z. Using laser ablation inductively coupled plasma mass spectroscopy (LA-ICP-MS) to determine the provenance of the cobalt pigment of Qinghua porcelain

from Jingdezhen in Yuan Dynasty of China (1271-1368 AD). Ceram Int 2015, 41: 9878-9884. https://doi.org/doi:10.1016/j.ceramint.2015.04.064

[10] Zhu T, Zhang Y, Xiong H, Feng Z, Li Q, Cao B. Comparison of the Different Types of Qinghua Porcelain from Jingdezhen in the Yuan Dynasty of China (1271-1368 AD) by Micro X-ray Fluorescence Spectroscopy (μ-XRF) and Microscopy. Archaeometry 2016; 58: 966-978. https://doi.org/doi:10.1111/arcm.12215

[11] Wang L, Wang C.S. Co speciation in blue decorations of blue-and-white porcelains from Jingdezhen kiln by using XAFS spectroscopy. J Anal At Spectrom 2011; 26: 1796-1801. https://doi.org/10.1039/c0ja00240b

[12] Figueiredo M, Silva T, Veiga J. A XANES study of cobalt speciation state in blue-and-white glazes from 16th to 17th century Chinese porcelains. J Electron Spectroscop 2012; 185: 97-102. https://doi.org/10.1016/j.elspec.2012.02.2007

[13] Qu X, Xu J, Xi X, Huang C, Yang J. Microstructure characteristics of blue-and-white porcelain from the folk kiln of Ming and Qing Dynasties. Ceram Int 2014; 40: 8783-8790. https://doi.org/10.1016/j.ceramint.2014.01.100

[14] Kock L, De Waal D. Raman studies of the underglaze blue pigment on ceramic artefacts of the Ming dynasty and of unknown origins. J Raman Spectrosc 2007; 38: 1480-1487. https://doi.org/10.1002/jrs.1805

[15] Jiang X, Ma Y, Chen Y, Li Y, Ma Q, Zhang Z, Wang C, Yang Y. Raman analysis of cobalt blue pigment in blue and white porcelain. A reassessment. Spectroc Acta A 2018; 190: 61-67. https://doi.org/10.1016/j.saa.2017.08.0767

[16] Wu J, Li J, Guo J. Microstructure study of color spots of Jingdezhen blue and white porcelain. J Inorg Mater 1999; 14: 143-149.

[17] Beijing wenwu yanjiusuo. Excavation Report on a Ming Period Burial at Maojiawan. Beijing: Kexue chubanshe; 2007.

[18] D'Ippolito V, Andreozzi G, Bersani D, Lottici P. Raman fingerprint of chromate aluminate and ferrite spinels. J Raman Spectrosc 2015; 46: 1255-1264. https://doi.org/10.1002/jrs.4764

[19] Ospitali F, Sabeta T, Tullini F, Nannetti M, Di Lonardo G. The role of Raman microspectroscopy in the study of black gloss coatings on Roman pottery. J Raman Spectrosc 2005; 36: 18-23. https://doi.org/10.1002/jrs.1259

[20] Bouchard M, Gambardella A. Raman microscopy study of synthetic cobalt blue spinel used in the field of art. J Raman Spectrosc 2010; 41: 1477-1485. https://doi.org/10.1002/jrs.2645

[21] Sarma S, Simons B, Joder HJ. Raman study of anorthite, calcium Tschermak's pyroxene, and gehlenite in crystalline and glassy states. Am Mineral 1983; 68: 1113-1125.

[22] De Waal D. Raman investigation of ceramics from 16th and 17th century Portuguese shipwrecks. J Raman Spectrosc 2004; 35: 346-349. https://doi.org/10.1002/jrs.1210

[23] De Waal D. Raman analysis of underglaze pigments on porcelain art. J Raman Spectrosc 2007; 38: 956-957. https://doi.org/10.1002/jrs.1717

[24] Kock, L. Raman spectroscopic studies of the underglaze pigments of porcelain shards of archaeological origins. Chemistry Thesis, Pretoria: Faculty of Natural and Agricultural Sciences of the University of Pretoria; 2009.

[25] Widjaja E, Hong Lim G, Lim Q, Mashadi A, Garland M. Pure component Raman spectral reconstruction from glazed and unglazed Yuan, Ming and Qing shards: a combined Raman microscopy and BTEM study. J Raman Spectrosc 2011; 42: 377-382. https://doi.org/10.1002/jrs.2721

[26] Carter E, Wood M, De Waal D, Edwards G. Porcelain shards from Portuguese wrecks: Raman spectroscopic analysis of marine archaeological ceramics. Herit Sci 2017; 5: 17. https://doi.org/10.1186/s40494-017-0130-9

[27] Bosi F, Halenius U, D'Ippolito V, Andreozzi G. Blue spinel crystals in the $MgAl_2O_4$-$CoAl_2O_4$ series: Part II. Cation ordering over short-range and long-range scales. Am Miner 2012; 97: 1834-1840. https://doi.org/10.2138/am.2012.4139

[28] Llusar M, Forés A, Badenes J, Calbo J, Tena M, Monrós G. Colour analysis of some cobalt-based blue pigments. J Eur Ceram Soc 2011; 21: 1121-1130. https://doi.org/10.1016/S0955-2219(00)00295-8

[29] Fernandez A, De Pablo L. Formation and the Color Development in Cobalt Spinel Pigments. Pigm Resin Technol 2002; 31: 350-356. https://doi.org/10.1108/03699420210449043

[30] Cavalcante P, Dondi M, Guarini G, Raimondo M, Baldi G. Colour performance of ceramic nano-pigments. Dyes Pigm 2009; 80: 226-232. https://doi.org/10.1016/j.dyepig.2008.07.004

[31] D'Ippolito V, Andreozzi G, Bosi F, Halenius U. Blue spinel crystals in the $MgAl_2O_4$-$CoAl_2O_4$ series: Part I. Flux growth and chemical characterization. Am Miner 2012; 97: 1828-1833. https://doi.org/10.2138/am.2012.4138

[32] Srisawad N, Chaitree W, Mekasuwandumrong O, Praserthdam P, Panpranot J. Formation of $CoAl_2O_4$ Nanoparticles via Low-Temperature Solid-State Reaction of Fine Gibbsite and Cobalt Precursor. J Nanomater 2012: 1. https://doi.org/10.1155/2012/108369

[33] Melo D, Cunha J, Fernandes J, Bernardi M, Mela M, Martinelli A. Evaluation of $CoAl_2O_4$ as ceramic pigments. Mater Res Bull 2003; 38: 1559-1564. https://doi.org/10.1016/S0025-5408(03)00136-3

[34] Zayat M, Levy D. Blue $CoAl_2O_4$ Particles Prepared by the Sol−Gel and Citrate−Gel Methods. Chem Mater 2000; 12: 2763-2769. https://doi.org/10.1021/cm001061z

[35] Ahmed I, Shama S, Moustafa M, Dessouki H, Ali A. Synthesis and spectral characterization of $Co_xMg_{1-x}Al_2O_4$ as new nano-coloring agent of ceramic pigment. Spectro Acta A 2009; 74: 665-672. https://doi.org/10.1016/j.saa.2009.07.024

[36] Duan X, Pan M, Yu F, Yuan D. Synthesis, structure and optical properties of $CoAl_2O_4$ spinel nanocrystals. J Alloys Compd 2011; 509: 1079-1083. https://doi.org/10.1016/j.jallcom.2010.09.199

[37] Salem S, Bondioli, F. Evaluation of green and blue cobalt aluminate spinels, http://www.nanoparticles.ch/archive/2012_Salem_PO.pdf ; 2012 [accessed 20 December 2019]

[38] Deer W, Howie R, Zussman J. An introduction to the rock-forming minerals. 2nd edition. Harlow: Longman Scientific & Technical; 1992.

[39] Torkian L, Daghighi M, Boorboor Z. Simple and Efficient Rout for Synthesis of Spinel Nanopigments. J Chem 2013: ID 694531. https://doi.org/10.1155/2013/694531

[40] Khattab R, Sadek H, Gaber A. Synthesis of $Co_xMg_{1-x}Al_2O_4$ nanospinel pigments by microwave combustion method. Ceram Int 2017; 43: 234-243. https://doi.org/10.1016/j.ceramint.2016.09.144

[41] Fahlman B. Materials Chemistry. Dordrecht: Springer; 2007.

[42] Möncke D, Papageorgiou M, Winterstein-Beckman A, Zacharias N. Roman glasses coloured by dissolved transition metal ions: redox-reactions, optical spectroscopy and ligand field theory. J Archaeol Sci 2014; 46: 23-36. https://doi.org/10.1016/j.jas.2014.03.007

[43] Green L, Hart A. Colour and chemical composition in ancient glass: An examination of some Roman and Wealden glass by means of ultraviolet-visible-infra-red spectrometry and electron microprobe analysis. J Archaeol 1987; 14: 271-282. https://doi.org/10.1002/jrs.5358